New Simplified Algorithm for the Multiple Rotating Frame Approach in Computational Fluid Dynamics

Lakhdar Remaki

Research Professor, Member of ASME

BCAM

Basque Center for

Applied Mathematics

Alameda Mazarredo 14, 48009

Bilbao, Spain

Email: lremaki@bcamath.org

Associate professor,

Department of Mathematics

and Computer Science

Alfaisal University

Riyadh, KSA.

Ali Ramezani

BCAM researcher BCAM

Basque Center for

Applied Mathematics

Alameda Mazarredo 14, 48009

Bilbao, Spain

Email: aramezani@bcamath.org

Jesus Maria Blanco

Professor, Member of ASME

University of the Basque Country

Alameda Urquijo s/n 48013

Bilbao, Spain

Email: jesus.blanco@upv.net

Imanol Garcia

PhD Student

BCAM

Basque Center for

Applied Mathematics

Alameda Mazarredo 14, 48009

Bilbao, Spain

Email: igarcia@bcamath.org

ABSTRACT

This paper deals with rotating effects simulation of steady flows in turbomachinery. To take into account the rotating nature of the flow,the frozen rotor approach is one of the widely used approaches. This technique, known in a more general context as a multiple rotating frame (MRF), consists on building axisymmetric interfaces around the rotating parts and solve for the flow in different frames (static and rotating). This paper aimed to revisit this technique and propose a new algorithm referred to it by a virtual multiple rotating frame (VMRF). The goal is to replace the geometrical interfaces (part of the Computer Aided Design (CAD)) that separate the rotating parts are replaced by a virtual ones created at the solver level by a simple user input of few points locations and/or parameters of basic shapes. The new algorithm renders the MRF method easy to implement, especially for edge-based numerical schemes, and very simple to use. Moreover it allows avoiding any re-meshing (required by the MRF approach) when one needs to change interface position, shape or simply remove or add new one, which frequently happened

in practice. Consequently, the new algorithm reduces sensibly the overall computations cost of a simulation. This work is an extension of a first version published in an ASME conference, and the main new contributions are the detailed description of the new algorithm in the context of cell-vertex finite volume method, and the validation of the method for viscous flows and the three-dimensional case which is of a big importance to the method to be attractive for real and industrial applications.

Nomenclature

V Volume of computational domain, m^3

ρ Density, kg/m^3.

u_i Velocity components, m/s.

E Total energy per unit mass, $N.m/kg$.

e Internal energy per unit mass, $N.m/kg$.

p Pressure, N/m^2.

δ_{ij} The Kronecker delta.

γ The ratio of specific heats.

A Area vector, m^2.

n Face normal vector.

Γ_I^J Points to a facet which connects node I to J.

ω Angular velocity vector, $1/s$.

ε_{ij}^k The Levi-Civita symbol.

Ω_I Dual mesh domain.

H Normal vector of the rotation axis.

OP Vector from the rotation axis position to an arbitrary point P inside domain.

superscripts:

r Property in relative frame.

α Dimension index (x, y, z).

subscripts:

IJ Nodes id

$ijkl$ indices to be used for Levi-Civita symbol $\{0,1,2\}$

The primary text heading is boldface and flushed left with the left margin. The spacing between the text and the heading is two line spaces.

1 Introduction

Simulating rotating effects is a major concern in many applications where fluid dynamics play a sensitive role. For instance, in turbomachinery, accurate and cost effective simulation of vortex flow caused by fixed and rotating frames interaction is a widely studied problem. Such machines are extensively used in many industries including aerospace [1–5], automotive [6–8] ventilation [9], power generation [10], chemical manufacturing [11], petroleum exploration [12] and others. This demonstrates the importance of turbomachines optimal design which should be based on a realistic flow simulation. Many techniques to simulate rotating effects have been developed in the literature including the single rotating frame method, multiple rotating frame method, sliding mesh method and so on. The multiple rotating frame (MRF) technique [13, 14], known as well as a frozen-rotor approach in turbomachinery, is one of the widely used for steady flows simulations. The technique consists of creating a physical interface between rotating and static parts of the geometry, then solve the Navier-Stokes equations in a relative frame (associated to the rotating part) and in a stationary frame. Information is transferred through the interface between different zones. In it current version, the method is not easy to implement and to use; first of all we need to create the interface at the CAD level which is not always an easy task, in particular for strongly connected rotating and static parts.Then we need to use a mesher capable to mesh more than one sub-domain. Note that the interface has no physical meaning, it is created for a numerical simulation considerations only. Indeed, instead of rotating physically the parts, a change of reference is applied leading to a resolution of two different sets of equations (in stationary and rotating frame) at both sides of the interfaces. As a consequence there is no need to any mesh movement, but of course only steady states could be simulated by such approach. One of major criticism of the method is that the interface position can affect the results accuracy and convergence [15]. The optimal position is unfortunately not trivial and could not be accurately defined before running the simulation. Therefore we may need to adjust the position of the interface at the CAD level and remesh the domain many

times. To overcome these shortcomings, we propose in this paper a simplified version (algorithm) of the MRF, we refer to it by VMRF (virtual multiple rotating frame). In this version one single mesh is used and the interfaces are created virtually at the solver level rendering the method in one hand easy to implement, indeed, no need of different meshes as in the classical MRF, that requires modifying the data structure of existing codes, and no need to implement interpolation methods at the interface of different domains. In the other hand, it is very easy to use, since no need to create the interfaces at the CAD level which could be a tricky task in case of strong connection between rotating and non-rotating parts of the geometry, and finally any adjustment of the interfaces is straightforward by a simple modification in the solver input data, therefore no need to modify the CAD and remesh the geometry reducing sensibly the computational cost. Moreover the VMRF provides a possibility of designing an automatic interface position adjustment algorithm during simulation.

This work is an extension of a first version published in an ASME proceedings [16]. The extensions consist of; first, the implementation details of the new algorithm in the context of cell-vertex finite volume method is provided showing that in this context it is quite straightforward. Then the virtual interface structure and the impact of mesh resolution is discussed. Finally a validation in three dimensional case is performed, which is crucial for the the algorithm to be attractive for a real and industrial applications, and its extension to viscous flows is implemented and tested on a 2D centrifugal pump. Note that in the conference paper a preliminary 3D test is shown to only demonstrate that the rotating mechanism is simulated but no validation is achieved. For the validation of the proposed algorithm, both methods, VMRF and the classical MRF (using a multizone approach) are implemented in BBIPED (Bcam-industrial platform for engineering design), a CFD opensource platform being developed using open source SALOME (grid generator) [17] and SU2 (CFD solver) [18] as library (http://www.bcamath.org/en/research/lines/CFDMS/software). Numerical tests are performed and results of both methods are compared. In some cases commercial code results and experimental data are provided.

2 Governing Equations

For the sake of simplicity only the Euler formulation will be used even if for the testing part of the paper the proposed algorithm is extended to viscous flows. The averaged equations governing three

dimensional compressible inviscid flow are formulated relative to a Cartesian (x_1, x_2, x_3) coordinate system, over a fixed volume V with a closed surface S, in the integral form as.

$$\frac{\partial}{\partial t}\int_V \vec{Q} dV = \int_S \vec{F}^{\alpha}(\vec{Q})\vec{n}_{\alpha} dS \quad \text{for } \alpha = 1, 2, 3 \tag{1}$$

where the summation convention is employed and $\vec{n} = (n_1, n_2, n_3)$ denotes the unit outward normal vector to S. In this equation,the conservative variables $\vec{Q}$ and the inviscid flux vectors $\vec{F}^{\alpha}$ are defined respectively by:

$$\vec{Q} = \begin{pmatrix} \rho \\ \rho u_1 \\ \rho u_2 \\ \rho u_3 \\ \rho E \end{pmatrix} \qquad \vec{F}^{\alpha} = \begin{pmatrix} \rho u_{\alpha} \\ \rho u_1 u_{\alpha} + p\delta_{\alpha,1} \\ \rho u_2 u_{\alpha} + p\delta_{\alpha,2} \\ \rho u_2 u_{\alpha} + p\delta_{\alpha,3} \\ (\rho E + p)u_{\alpha} \end{pmatrix} \tag{2}$$

where ρ and p denote the averaged density and pressure of the fluid respectively and $E = e + \frac{1}{2}(u_{\alpha}u_{\alpha})$ is the total energy per unit mass, with e being the internal energy per unit mass for the fluid, u_{α} is the averaged velocity of the fluid in direction x_{α} and $\delta_{\alpha,i}$ is the Kronecker delta.

The equation set is closed by the addition of the ideal gas equation of state (i.e. $p = \rho(\gamma - 1)e$, where ρ is the density and γ is the ratio of specific heats). Steady state solutions of the resulting equation set are defined in a fixed spatial computational domain Ω.

3 Numerical Discretisation

To discretize the Euler equations described above a cell-centred finite volume method is used. In the following we give a short review of the method and for more details see [19].

On the generated consistent mesh, nodes are located at the vertices of the elements and the spatial

discretisation of equation (1) is accomplished by using a cell vertex finite volume method [19]. This requires the construction of a dual mesh, in which each cell is associated with a single node of the primal mesh. For those regions in which the primal mesh consists only of isotropic tetrahedral cells, a median dual mesh is built by connecting cell edge midpoints, cell centroids and cell face centroids, such that only one node is present within each dual mesh cell [20–22]. With this strategy, each node I of the domain mesh is associated with a volume Ω_I of the dual mesh. The boundary surface of such volume is denoted by Γ_I. Each edge of the domain mesh is associated with a segment of the dual mesh interface between the nodes connected to the edge. This segment is a surface built from triangular facets, where each facet is connected to the midpoint of the edge, a neighboring element centroid and the centroid of an element face connected to the edge, as illustrated in Fig. 1 (a). The midpoint of the edge between node I and J is denoted by $\vec{x}_m^{IJ}$, the centroid of the face with vertices I, J and K is denoted by $\vec{x}_s^{IJK}$ and the element centroid is designated by $\vec{x}_c$. The bold lines on the dual mesh in this figure illustrate the boundaries between the edges in which the dual mesh segment is associated with. For this dual mesh definition, the volume Ω_I can be viewed as being constructed in terms of a set of tetrahedra, as illustrated for a typical interior node I in Fig. 1 (b). The surface of the dual mesh cell surrounding node I is defined in terms of the closed set of planar triangular facets Γ_I^K, where each facet only touches a single edge of the domain mesh. The set of facets matching the edge between nodes I and J is denoted by Γ_{IJ}.

In general, the median dual approach cannot be used for the hybrid elements produced by merging the stretched tetrahedra generated by the advancing layers method. This is because cells created in this way may be warped so severely that a vertex can lie outside the corresponding median dual cell. This may occur in regions of high curvature or at the interface between the hybrid and isotropic meshes. To overcome this problem, the information contained in the primal tetrahedral mesh is used to ensure that topology of the control volume cells is valid [20, 23]. Equation (1) is applied to each cell Ω_I of the dual mesh. To perform the numerical integration of the inviscid fluxes over the surface Γ_I of this cell, a set of coefficients is calculated for each edge using the dual mesh segment associated to the edge. The values of these coefficients for an internal edge are evaluated as [21, 22]

$$A_{IJ}^{\alpha} = \sum_{K \in \Gamma_{IJ}} A_{\Gamma_I^K} n_{\Gamma_I^K}^{\alpha} \tag{3}$$

where $A_{\Gamma_I^K}$ is the area vector of facet Γ_I^K and $n_{\Gamma_I^K}^{\alpha}$ is the component, in direction x_α, of the outward unit normal vector of the facet from the viewpoint of node I. The integral of the inviscid flux over the surface Γ_I is then approximated, using the summation of edge contributions, as [22]

$$\int_{\Gamma_I} \vec{F}^{\alpha} d\Gamma \approx \sum_{J \in \Lambda_I} \tilde{\vec{F}}_{IJ} A_{IJ}^{\alpha} \tag{4}$$

where Λ_I denotes the set of nodes connected to node I by an edge in the domain mesh. Here,

$$\tilde{\vec{F}}_{IJ} = \begin{pmatrix} \rho q_{IJ} \\ \rho u_1 q_{IJ} + p n_{IJ}^1 \\ \rho u_2 q_{IJ} + p n_{IJ}^2 \\ \rho u_3 q_{IJ} + p n_{IJ}^3 \\ (\rho E + p) q_{IJ} \end{pmatrix} \tag{5}$$

is a consistent numerical inviscid flux function and

$$q_{IJ} = n_{IJ}^{\alpha} \left(u_\alpha\right)_I \tag{6}$$

is the velocity in the direction of the edge connecting nodes I and J. The fluxes are estimated using a second order HLLC Riemann solver and indefinitely differentiable limiters as in [24,25]. For low Mach, however, the code switches automatically to Roe-Turkel solver [26] which uses a local preconditioning in order to obtain a truncation error depending only on h not h/M making the solution more stable. The

solution is advanced in time to steady state using an explicit multi-stage Runge Kutta procedure and an implicit time stepping with biconjugate gradient stabilized solver. The convergence is accelerated by the use of local time stepping and by the addition of an agglomerated multigrid process.

4 Multi-zones approach for multiple rotating frame method (MRF)

Before describing the proposed VMRF algorithm, first we give a short reminder of the Multiple Rotating Frame (MRF) [13, 18] approach and its implementation through the Multi-zones domain decomposition technique. Note that actually the flow for such problems is unsteady due to the existence of fixed (ex. volute) and rotating parts (ex. rotor) simultaneously in the domain. The MRF technique however, by putting the observer on the rotating axis, allows to view the problem as steady. The observer of the rotating domain will feel a steady state so any unsteadiness in boundaries violates the validity of the MRF assumption [27]. Therefore the definition of the interface which is the outer boundary of the rotating part is very important and misplacing it may lead to divergence or appearance of non physical phenomena [28]. This approach consists of defining an axisymmetric sub-domain containing the rotating part endowed with a relative frame. The Euler equations are expressed in the relative frame to simulate rotating parts (in which they are considered static), while a stationary frame is used for the rest of the domain. A steady transfer of information is made through the interface separating the two domains. The Euler equations in the rotating frame are given by:

$$\frac{\partial}{\partial t}\int_V \vec{Q}^r\, dV = -\int_S \vec{F}^{\alpha}(\vec{Q}^r)\, n_\alpha\, dS + \int_V \vec{S}\, dV \quad \text{for } \alpha = 1, 2, 3 \tag{7}$$

$$\vec{S} = \begin{pmatrix} 0 \\ -2\varepsilon 1 i j \omega u^r - \varepsilon^1_{kl}\varepsilon^k_{ij}\omega_i x_j \omega_l \\ -2\varepsilon 2 i j \omega u^r - \varepsilon^2_{kl}\varepsilon^k_{ij}\omega_i x_j \omega_l \\ -2\varepsilon 3 i j \omega u^r - \varepsilon^3_{kl}\varepsilon^k_{ij}\omega_i x_j \omega_l \\ 0 \end{pmatrix} \qquad \vec{Q}^r = \begin{pmatrix} \rho \\ \rho u^r_1 \\ \rho u^r_2 \\ \rho u^r_3 \\ \rho E^r \end{pmatrix} \tag{8}$$

$$u^r_\alpha = u_\alpha - \varepsilon\alpha i j \omega x \qquad E^r = e + \frac{1}{2}(u^r_\alpha u^r_\alpha - \varepsilon^\alpha_{ij}\varepsilon^\alpha_{kl}\omega_i x_j \omega_k x_l) \tag{9}$$

where ε^i_{jk} is Levi-Civita symbol and r superscript refers to the relative frame. ω is the angular velocity vector and x is the Cartesian position vector of the cell, P_r e, U_r denote the averaged density, pressure, total energy and velocity of the fluid in the rotating frame respectively. $2\varepsilon\alpha i j \omega u^r$ and $\varepsilon^\alpha_{kl}\varepsilon^k_{ij}\omega_i x_j \omega_l$ are the *Coriolis* and centripetal forces respectively.

The multi-zones strategy to implement the MRF method, consists on splitting the geometry into several zones meshed independently and communicate through interfaces by variables or fluxes exchange. Note that this approach allows to handle many complex situations and not restricted to the case of rotating parts of a given geometry. Back to the MRF case, the interface vertices belong to two different zones, rotating and stationary. The control volume for duplicated vertices (on the interface) should be the same, resulting in an automatic matching of the solution of both zones. In Fig. 2 the residual of the lower part of the control volume is calculated by the lower zone and the upper part by the upper zone without shared information, then these residuals are added to both zones. We refer to this approach as the flux exchange scheme. In the second approach the residual of each part is calculated taking into account the dotted faces (in Fig. 2) which brings information from the other zone and updated independently. The conservative variables values are exchanged (at the dotted faces) implicitly between the two parts of the control volume. In this approach it is not guaranteed that the flow properties on common nodes to be identical. The advantage of this approach is that each zone preserves its autonomy and also it is suitable

for zones that have common faces but not necessarily common nodes. This situation always happens in sliding meshes or mixing planes or in some overset grids approaches. We refer to this approach as the variable exchange scheme.

5 Virtual Multiple Rotating Frame (VMRF)

As mentioned in the introduction, the MRF method described above is not easy to implement and to use since it requires creating boundaries (representing the interfaces) at the CAD level which could be a tricky task in many cases where the rotating parts are connected in a complex way to stationary parts. The mesher used should be able to generate a grid with more than one closed domain and this could not be achieved by meshers using a simple Delaunay strategy for instance. Even if nowadays moderm meshers could achieve such a task, it is still not the case for many simple mesh generators. Finally and maybe the most restricting drawback is the need of remeshing when the interface is not correctly located or defined since the CAD needs to be modified. This results in a sensitive increase of the computational cost. To simplify the method and avoid all these constraints, we propose a new algorithm to achieve the MRF technique by building a virtual interface at the solver level rather than a physical interface at the CAD level. The virtual axisymmetric (Fig. 3) zone containing the rotating domain is defined at the solver input and no need to split the mesh. Providing nodes location, and rotating axes, curves are created by a simple linear interpolation, then the virtual zone is obtained by revolving the curve as follows: Let f and g two interpolated curves as in (Fig. 3) and L the height of the zone, let a and b define by

$$a = OP_i\, H_i \quad \Rightarrow \quad b = \sqrt{(OP_i - aH_i)(OP_i - aH_i)} \tag{10}$$

where H represents the rotation axis, O the rotating center, and P an arbitrary point, the relative coordinate being OP. The node is inside the zone if and only if

$$f(a) < b < g(a) \text{ and } a < L$$

For the simulations performed in this work curves are straight lines, the virtual zone is then a cylinder and no need to provide nodes location but only rotating axes, center and the height of the cylinder. Note that complex interfaces could be obtained by simply assembling simple geometries like cylinders, cones, spheres and so on.

5.1 VMRF for the cell-centred finite volume

In this subsection, the VMRF in the context of cell-centred and edge-based finite volume method is described. Recall that for this method fluxes are computed by looping on edges only. Therefore, the virtual interface is easily and entirely identified by edges that have one vertex in the rotating zone (cylinder) and the other outside as in Fig. 4. Consequently, only these edges need a special treatment to exchange fluxes. In another hand, the actual virtual interface is not the one defined by the user, which serves only as a guide to locate the nodes belonging to the rotating zone. It is the one obtained by assembling patches (Fig. 5) of the dual cells. As a results, the assembled virtual interface is not perfectly axisymmetric, this could be fixed for instance by refining the grid around this surface. However, and as we will see in the testing section, this is not necessary and has no influence on results.

Let's now give some more technical details of the methods. Recall that for the edge-based cell-centred finite volume method, to estimate the fluxes we loop on the edges and compute the contribution of each dual patch to the corresponding connected nodes by adding and subtracting. For edges that cross the interface two fluxes however are computed since one node is rotating and the other is static. This is done by converting the momentum and energy between the two frames. The momentum is converted by a simple frame change as fellows,

$$V_a = V_r + u_r \tag{11}$$

Where V_a is the velocity in the absolute (static) frame, V_r the relative velocity (the velocity in the rotating frame) and $u_r = \omega \times x$ is the frame rotating velocity. As for the energy this is less straightforward, but could be put in a simple formula as fellow,

First express the energy in both frames

$$E_a = h - \frac{p}{\rho} + \frac{1}{2}V_a^2 \qquad E_r = h - \frac{p}{\rho} + \frac{1}{2}(V_r^2 - u_r^2) \tag{12}$$

By identification we get

$$E_a = E_r + \frac{1}{2}(V_r^2 - V_a^2 - u_r^2) \tag{13}$$

By using (11) we obtain

$$E_r = E_a - \overrightarrow{V_a}.\overrightarrow{u_r} \tag{14}$$

Finally Coriolis and Centripetal forces are added to the Euler equations for nodes belonging to the virtual zone as a source term.

Note that for the rotating zone the absolute formulation of the Euler equation is used instead of (7), this is easier to implement especially in the case of Navier-Stokes equations since the viscous terms don't need to be modified. This formulation is given by,

$$\frac{\partial(\rho v)}{\partial t} = -\nabla.(\rho v_r v) - \rho(\omega \times v) - \nabla v + \nabla\tau + \rho g + F \tag{15}$$

Another important issue is the extension of the method to incompressible flows. The more straight forward way to achieve such extension is to use the Pseudo-compressibility formulation, in this case the equations still on the same nature, avoiding solving an elliptic problem for the pressure which will require to derive an adapted formulation for the VMRF. This means we solve the same equation (15) with a constant density and the continuity equation is kept where the density is replaced by P/β^2, with

P beying the static pressure and β the artificial compressibility constant, see [29] for details.

Let's now summarize the VRMF algorithm in the context of edge-based cell-vertex finite volume method

The Algorithm:

1. Identify the nodes belonging to the rotating domain as described above

2. When looping on edges

   (a) Identify those for which both nodes are not rotating and do no modifications

   (b) Identify those for which both nodes are rotating and only add Coriolis and centrifugal forces as source term without any change to the fluxes

   (c) Identify those for which one node is rotating and one is not rotation then transfer the fluxes by converting the momentum and energy from the rotating frame to the absolute one and vice versa.

6 Numerical tests

To assess and validate the proposed VMRF algorithm a 2D and 3D test cases are considered. A 2D first test case is designed to include all basic aspects of turbomachinery including rotating fan, fixed volute and mixing zone with high speed free stream (see Fig. 6). The 3D test case concerns the study of the aerodynamic behaviour of the well known HAWT (horizontal axis wind turbine) NREL Phase VI. This wind turbine was widely simulated showing the high complexity of the fluid behaviour (Fig. 9), and still a challenging numerical test to accurately match experimental data [30, 31]. For the last test case, the VMRF is extended and implemented for viscous flows, and a centrifugal pump is simulated to assess the behaviour of the new algorithm in the case of rotor-stator interaction with a small gap between

the impeller blades and diffuser vanes. Note that even if some results are compared to a commercial code and experimental data, the main objective of the tests is not to assess the performance of the MRF method which is widely studied in the literature, but to demonstrate that the new VMRF algorithm (that implements MRF),is providing the same accuracy as the MRF technique inheriting its well known positive and negative points, while bringing the various practical advantages developed along this paper. For visualization the opensource PARAVIEW is used.

6.1 Inviscid flow

6.1.1 2D case

This test consists of a rotating blades in a cavity representing a volute. The goal is to assess the behaviour of the VMRF compared to the MRF for a complex flow resulting from an interaction of a rotation fan with a close wall. For the simulation, the inlet (left side surface of the geometry) Mach number is set to 0.6, the fan angular speed is set to 150 rad/s. The right and top sides are considered as far-field, and the bottom side and the blades as walls on which slip condition is imposed. The flow is assumed to be inviscid and compressible. The domain is discretized by a full unstructured quads mesh containing 5889 nodes for the VMRF method and 5983 for the MRF. The simulation is repeated using VMRF, Multizone MRF implemented in BBIPED and Ansys-Fluent v. 14.5 (using MRF) [32] respectively. Due to the interaction of the free stream and the rotating fan a complex flow is observed which is depicted using streamlines and Mach contours in Fig. 6. The pressure contours of VRMF and Fluent are qualitatively compared in Fig. 7. for a quantitative comparison, the pressure distribution is extracted from a horizontal line (horizontal white line in Fig. 6), then it is plotted in Fig. 8. These figures show a good agreement of both VMRF and Multi-zone-MRF with the highly reliable commercial software Ansys-Fluent. Note that the slightly difference between the used meshes for MRF and VMRF (because we have two meshed zones for the first and a single mesh for the second) can explain the small discrepancy between the two algorithms. Indeed, the virtual interface, as we mentioned in the paper, is actually formed by patches of the dual mesh and then it is not a smooth surface. However, when we match the meshes as we can see in the next tests, the virtual interface coincides with the physical one (smooth surface/curve) and results perfectly agreed.

6.1.2 3D case

To validate the new algorithm in the 3D case, the NREL Phase VI wind turbine is selected. This is designed using a 5.5 m twisted blades with S809 airfoil. The tower is excluded in the CFD simulations since the turbine is upwind type and then this exclusion has no big effect on rotor aerodynamics calculations. The simulation conditions are; blades rotate at 72 rpm and the wind speed is set to 10.3 m/s. Note that these conditions are enough to cause stall, particularly at the middle of the blades. Since we deal with a low Mach flow, elliptical nature of the regime forces us to use a large domain to minimize the boundary effects on our results. The virtual rotating zone containing the blades is a cylinder as shown in (Fig. 10). The used mesh contains 272463 nodes and 1384084 elements. The blades are discretized with a structured grid to better capture curvatures, and unstructured grid is used for the rest of the domain (See Fig. 11). For this test case we arranged to have a perfectly matched meshes for both algorithms. A far-field boundary condition is imposed to the cylinder domain, and slip condition is imposed to the blades. As in the previous test, the problem is solved with both VMRF and the classical Multi-zone-MRF algorithms. The cp curves at different sections ($r/R = 30$ %,$r/R = 63.3$ % and $r/R = 95$ %) are shown in Fig. 12 for both approaches. we can see that we have a perfect agreement of the curves, which demonstrate the validity of the new algorithm. Note that and as we claimed in this paper, there is no need to refine the mesh in order to define a smooth virtual interface. Indeed and as we can see in Fig. 11 the mesh is quite coarse at the virtual interface location.

Finally and despite that we simulated inviscid flow and it is not the goal of the paper, we find it worth to show a comparison of the VRMF to experimental data that are, and as we mentioned before, very difficult to match because of the stall problem. It is reported in ([30]) that the provided airfoil profile has a truncated trailing edge so there are two pressure values at approximately the same location. The obtained results shown in Fig. 13, are comparable to ones published in [30] and [33] and of course by solving the full Navier-Stokes we expect get better results.

6.2 Viscous flow

For the last test and to validate the new algorithm for viscous flows and in the case of rotor-stator interaction with a small gap, the method is first extended and implemented for viscous flows. Then

a 2D simplified model of an unshrouded centrifugal pump is selected. This is a seven blades and a radial vaned diffuser with 12 vanes pump presenting a small radial gap between the impeller blades and diffuser vanes, see Fig. 14. This small gap results in a highly unsteady flow. Of course in our case the flow is considered steady and the goal is to compare the VMRF and MRF in such extreme conditions. The simulation is performed for the rotating speed of 2000 rpm, and inlet (inner circle) velocity of 12.5 m/s. The domain is inscribed in a circle of 35 centimetre radius considered as far-field. Spalart-Allmaras turbulence model is used. Unstructured single mesh is generated for the VMRF algorithm containing 17993 nodes and a two zones unstructured mesh of 18167 nodes is generated for the MRF algorithm. Fig. 15 shows a zoom on the MRF and VMRF meshes, we can see that the physical interface is replaced by a virtual one for the VMRF that crosses the mesh elements which could complicate the method if an element centred finite volume is used since we will need to track the surface to estimate the fluxes. However for the cell-vertex method we use in this paper, this is naturally handled, as we mentioned before, by the dual mesh and no need to track the virtual surface. The streamlines of both methods are depicted in figures Fig. 16 and Fig. 17 for non-matched and matched meshes, this is visualized by using the line option in PARAVIEW, and we selected two lines that is why only two recirculation zones are appearing. The results show a quite identical solutions for the matched meshes and small difference is noticeable for the non-matched one, due indeed to the mesh difference as in the previous tests. To complete the comparison pressure profiles along a curve located on the impeller outlet midspan are depicted for both methods and shown in Fig. 18. The results confirm the perfect agreement for matched meshes and a small discrepancy but good agreement for non-matched meshes. We finally conclude that the VMRF is reproducing the MRF results in a reliable way as demonstrated by the different kind of simulations we performed in this work.

7 Conclusions

In this paper a new algorithm (VMRF) to simulate flow in rotating machines like turbomachinery is proposed. This is based on a modification of the well known multiple rotating frame (MRF) by building a virtual interface between the rotating and stationary parts of the domain using a single mesh, rather than creating interfaces at the CAD level and decomposing the domain in many meshed zones. The virtual interfaces are defined at the solver level by the mean of revolving curves or elementary geomet-

rical shapes. This turns the method much more easy to implement and to use, avoiding tricky tasks when building CAD interfaces for close and complex parts connections. Moreover no need to CAD modification and re-meshing when some interface adjustments are necessary (which usually happen) since this is done at the solver level by a small modification of the input file. And no need to generate many sub-meshes. This obviously reduces sensibly the processing time of the simulations and effort. This could as well open a door to some automatic algorithms for interface location adjustment during simulation.

The algorithm is explained in details in the context of cell-vertex finite volume method. It is implemented in BBIPED, a BCAM CFD platform and for the sake of validation the classical MRF using a multizone approach is implemented as well. A 2D fan and pump and 3D wind turbine tests cases are simulated demonstrating that the new algorithm despite its simplicity gives exactly the same answers as the MRF one, which makes it very attractive especially for industrial applications.

Acknowledgements

This research is supported by the Basque Government through the BERC 2014-2017 program and by the Spanish Ministry of Economy and Competitiveness MINECO: BCAM Severo Ochoa accreditation SEV-2013-0323. The authors gratefully acknowledge the financial support of Diputación Foral de Bizkaia (DFB) for this research and the whole BCAM-BALTOGAR project on turbomachinery (grant BFA/DFB-6/12/TK/2012/00020). Spanish Ministry of Economy and Competitiveness with reference MTM2013-40824-P. Alfaisal University grant IRG with reference IRG16413

References

[1] Adamczyk, J., 1998. "Numerical simulation of multi-stage turbomachinery flows". *RTO AVT Symposium On Design Principles and Methods for Aircraft Gas Turbine Engines*.

[2] Ekici, K., Hall, K., and Dowell, E., 2008.. "Computationally fast harmonic balance methods for unsteady aerodynamic predictions of helicopter rotors". *Journal of Computational Physics,,* **Volume 227,**(12), pp. 6206–6225.

[3] Oro, J. F., Gonzlez, J., Daz, K. A., and Coln, F., 2011. "Decomposition of deterministic unsteadiness in a centrifugal turbomachine: Nonlinear interactions between the impeller flow and volute

for a double suction pump". *Journal of Fluids Engineering,* **133**(1).

[4] Wang1, B., Okamoto, K., Yamaguchi, K. A., and Teramoto, S., 2014. "Loss mechanisms in shear-force pump with multiple corotating disks". *Journal of Fluids Engineering,* **136**(8).

[5] Zhongjie, L., Zhengwei, W., Xianzhu, W., and Daqing, Q., 2016. "Flow similarity in the rotorstator interaction affected region in prototype and model francis pump-turbines in generating mode". *Journal of Fluids Engineering*.

[6] Olander, M., 2011. "Cfd simulation of the volvo cars slotted walls wind tunnel". Master's thesis, Department of Applied Mechanics, Chalmers University of Technology,.

[7] Axerio-Cilies, J., and Iaccarino, G., 2012. "An aerodynamic investigation of an isolated rotating formula 1 wheel assembly". *Journal of Fluids Engineering,* **134**(12).

[8] Drian, T., Remaki, L., Fellouah, H., and Desrocher, S. M. A., 2013. "Aerodynamic study of a tricycle wheel sub-system for drag reduction". *Journal of Fluids Eng,* **136**.

[9] Califano, A., and Steen, S., 2009. "Analysis of different propeller ventilation mechanisms by means of rans simulations". In First International Symposium on Marine Propulsors, Trondheim, Norway,.

[10] Mirzamoghadam, A., Riahi, A., and Morris, M., 2012. "High pressure turbine low radius radial tobi discharge coefficient validation process". *Journal of Fluids Engineering,* **135**(7).

[11] Singh, K., Mahajanim, S., Shenoy, K., Patwardhan, A., and Ghosh, S., 2007. "Cfd modeling of pilot-scale pump-mixer: Single-phase head and power characteristics". *Chemical Engineering Science, Vol. 22, Issue 5, pp. 1308-1322,.*

[12] Wadnerkar, D., Utikar, R., Tade, M., and Pareek, V., 2012.. "Cfd simulation of solid?liquid stirred tanks". *Advanced Powder Technology, Volume 23, Issue 4, Pages 445-453,.*

[13] Luo, L., Gosman, A., and Issa, I., 1994.. "Prediction of impeller-induced flows in mixing vessels using multiple frames of reference". *Inst. Chem. Eng. Sympo. Ser., Vol. 136, 549-556,.*

[14] Warda, H., Wahba1, E., and Selim, E., 2014. "Integral pumping devices for dual mechanical seals: Experiments and numerical simulations". *Journal of Engineering for Gas Turbines and Power,* **137**(2).

[15] Zadravec, M., Basic, S., and Hribersek, M., 2007. "The influence of rotating domain size in a rotating frame of reference approach for simulation of rotating impeller in a mixing vessel".

Journal of Engineering Science and Technology, Vol. 2, No. 2, pp. 126 - 138,.

[16] Remaki, L., Ramezani, A., Blanco, J., and Antolin, J., 2014. "Efficient rotating frame simulation in turbomachinery". In ASME Turbo Expo 2014: Turbine Technical Conference and Exposition, Vol. 2B: Turbomachinery.

[17] , 2014. Salome Platform.

[18] Palacios, F., Colonno, M., Aranake, A., Campos, A., Copeland, S., Economon, T., Lonkar, A., Lukaczyk, T., Taylor, T., and Alonso, J., 2013.. "Stanford university unstructured (su2): An open-source integrated computational environment for multi-physics simulation and design". In AIAA Paper 2013-0287, 51st AIAA Aerospace Sciences Meeting and Exhibit. Grapevine, Texas, USA, January 7th - 10th,.

[19] Eymard, R., Gallouët, T., and Herbin, R., 2000. "Finite volume methods". *Handbook of numerical analysis,* **7**, pp. 713–1018.

[20] Sorensen, K., 2002.. "A multigrid accelerated procedure for the solution of compressible fluid flows on unstructured hybrid meshes". PhD thesis, University of Wales, Swansea,.

[21] Barth, T., 1995. *Aspect of unstructured grids and finite-volume solvers for the Euler and Navier-Stokes equations*. In Lecture Notes Presented at the VKI Lecture Series. Von karman Institute for fluid dynamics, 1994-05., Rhode Saint Genese Begium,, 02.

[22] Blazek, J., 2001. *Computational Fluid Dynamics: Principles and Applications*. Elsevier.

[23] Sorensen, K., Hassan, O., Morgan, K., and Weatherill, N., 2003. "A multigrid accelerated hybrid unstructured mesh method for 3d compressible turbulent flow". *Comp.Mech.,* **31**, pp. 101–114.

[24] Remaki, L., Hassan, O., and Morgan, K., 2010. "New limiter and gradient reconstruction method for hllc-finite volume scheme to solve navier-stokes equations". In ECCOMAS, the fifth European Congress on Computational in Fluid Dynamic, Lisbon, Portugal, pp. 14–17.

[25] Remaki, l., Hassan, O., and Morgan, K., 2011. "Aerodynamic Computations Using a Finite Volume Method with an HLLC Numerical Flux Function". *Mathematical Modelling of Natural Phenomena,* **6**(3), 1, pp. 189–212.

[26] Turkel, E., 1987. "Prcconditioned methods for solving thc incompressible and lowl sputd coninpressible equpations". *Jouirnal of Computational Physics,* **72**, pp. 277–298.

[27] Denton, J., 2010.. "Some limitations of turbomachinery cfd". In ASME Paper GT2010-22540,.

[28] Liu, Z., and Hill, D., 2000. "Issues surrounding multiple frames of reference models for turbo compressor applications". In International Compressor Engineering Conference, no. Paper 1369.

[29] Chorin, A., 1967. "A numerical method for solving incompressible viscous flow problems". *J. Comput. Phys,* **2**, pp. 12–26.

[30] Moshfeghi, M., Song, Y., and Xie, Y., 2012. "Effects of near-wall grid spacing on sst-k-omega model using nrel phase vi horizontal axis wind turbine". *Journal of Wind Engineering and Industrial Aerodynamics,,* **Volumes 107108**, AugustSeptember, pp. 94–105,.

[31] Hand, M., Simms, D., Fingersh, L., Jager, D., Cotrell, J., S.Schreck, and Larwood, S., 2001.. Unsteady aerodynamics experiment phase vi: Wind tunnel test configurations and available data campaigns.

[32] Ansys, 2014. Ansys fluent: Computational fluid dynamics simulator.

[33] Yelmule, M., and VSJ, E. A., 2013. "Cfd predictions of nrel phase vi rotor experiments in nasa/ames wind tunnel". *International journal of renewable energy research,,* **3**(2).

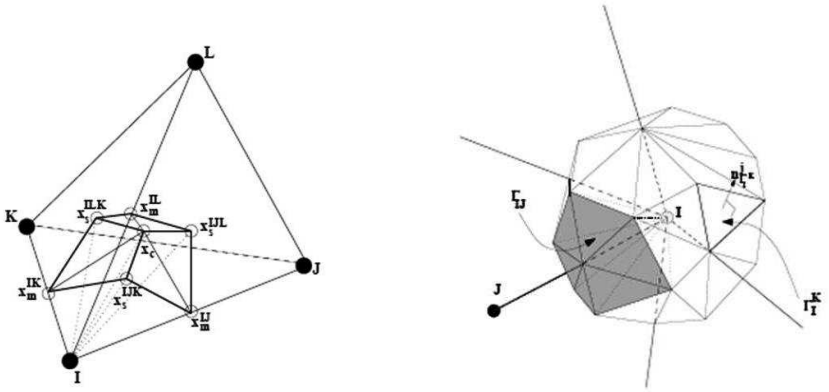

(*a*) (*b*)

Fig. 1: (a) Illustration of the part of the dual mesh cell surrounding node *I* within a tetrahedral cell. (b) Illustration of the dual mesh cell surrounding an internal node *I*.

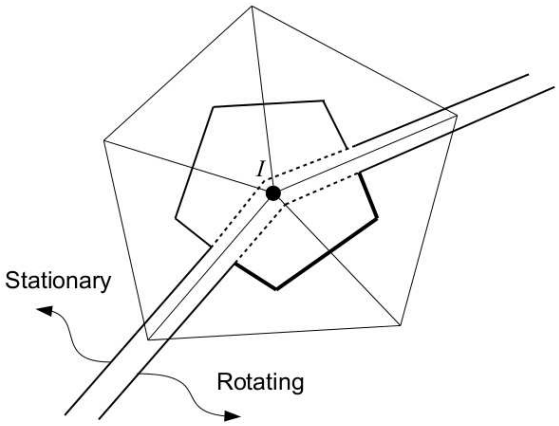

Fig. 2: Control volumes on matching nodes at the interface

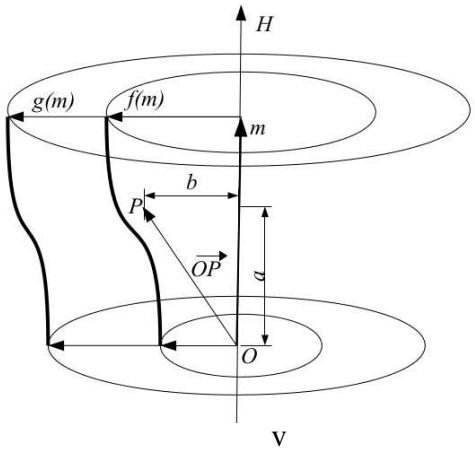

Fig. 3: Example of interfaces obtained by revolving curves

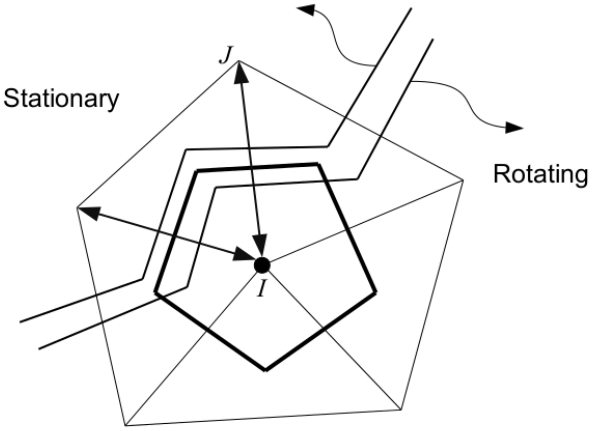

Fig. 4: Control Volume on virtual zones at the interface

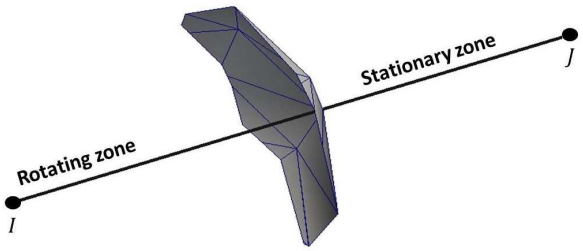

Fig. 5: The dual-cell interface separating rotating and static zones

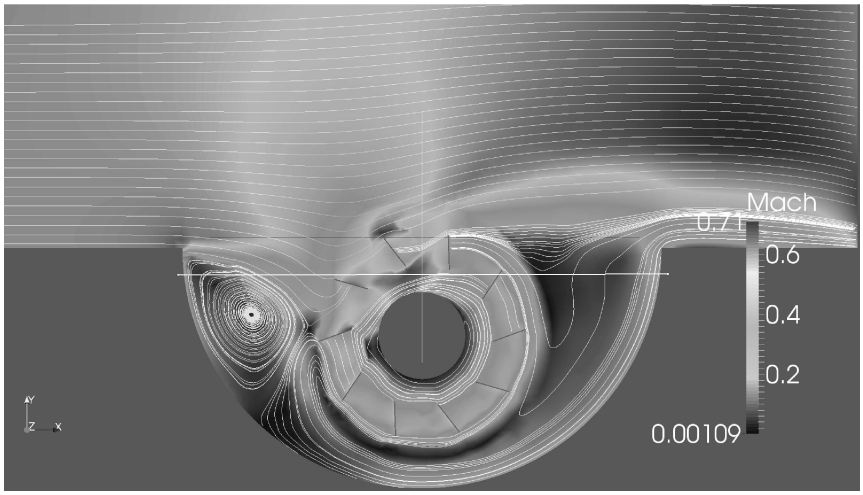

Fig. 6: VMRF simulation: Mach contours and streamlines.

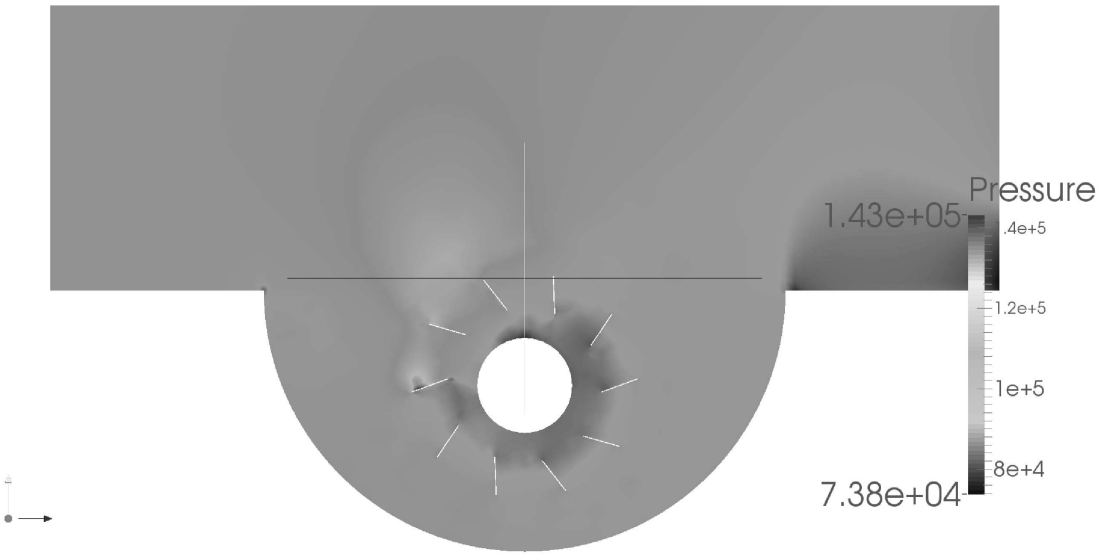

(*a*)

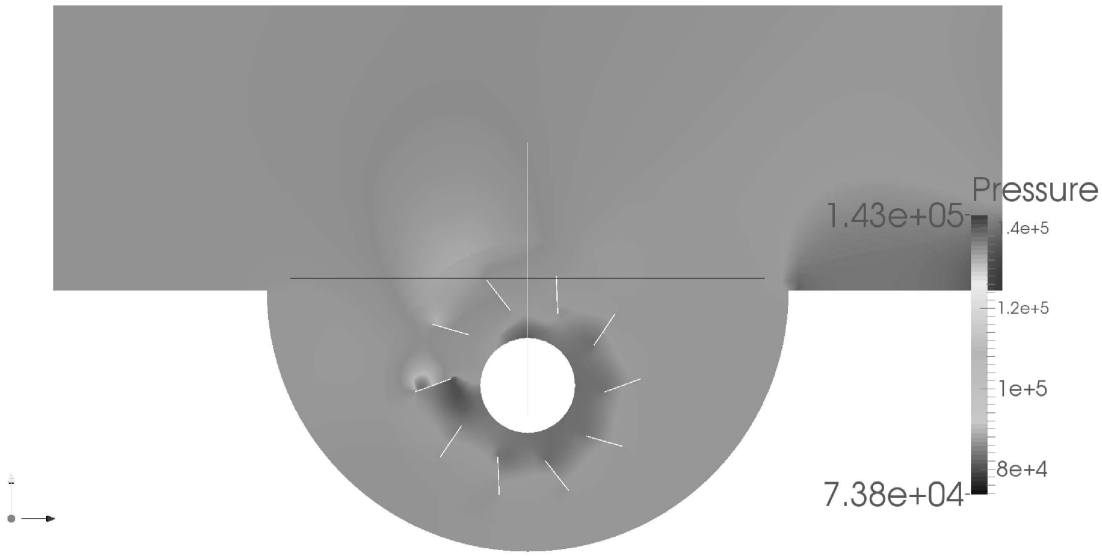

gs

(*b*)

Fig. 7: Pressure profile comparison: (a) FLUENT, (b) BBIPED.

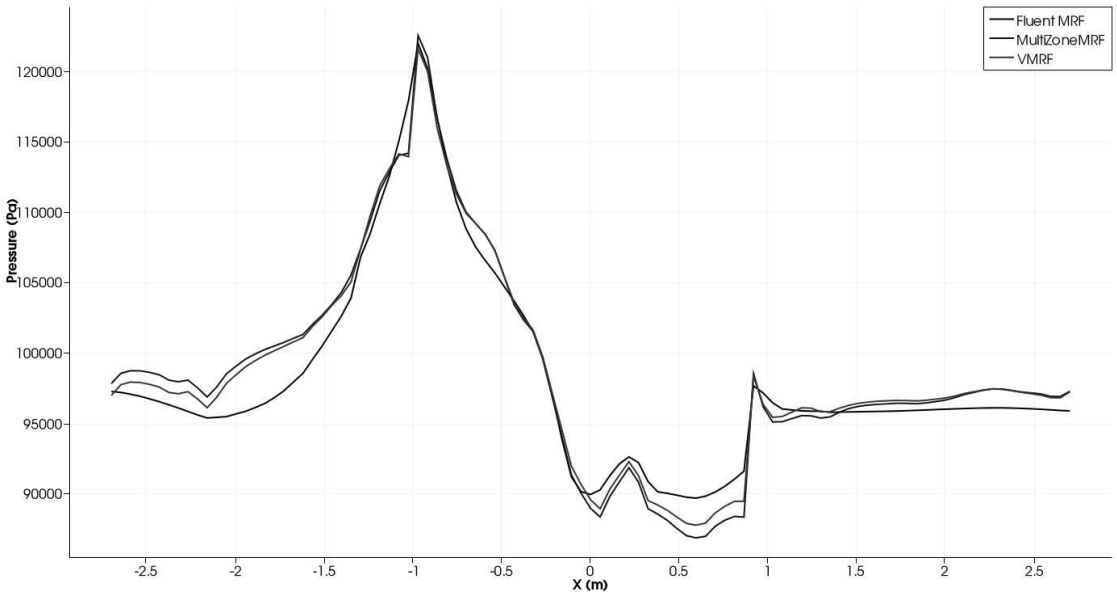

Fig. 8: Pressure profiles comparison along an arbitrary line

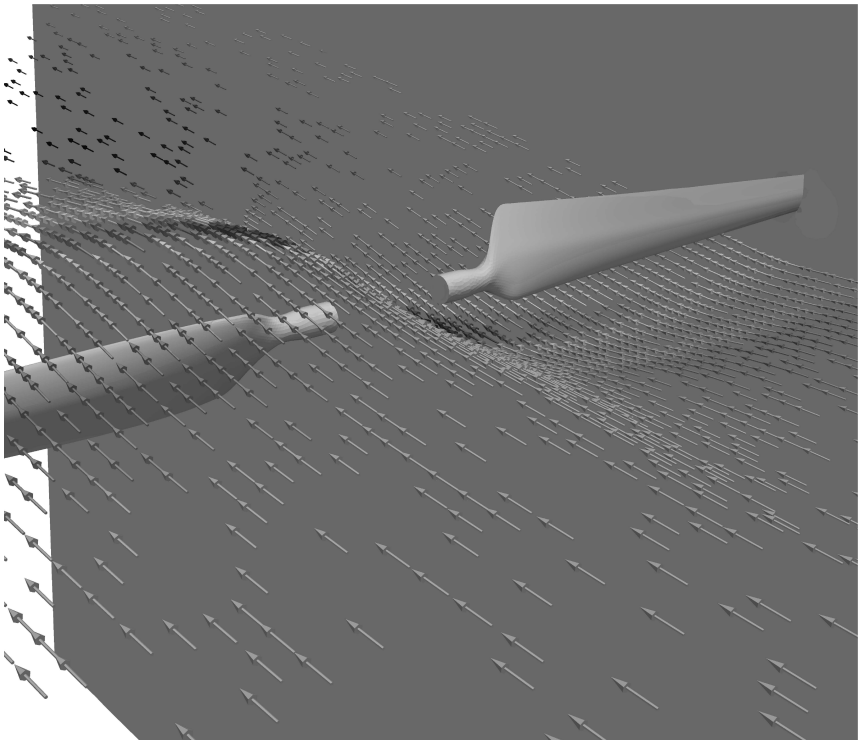

Fig. 9: Velocity field

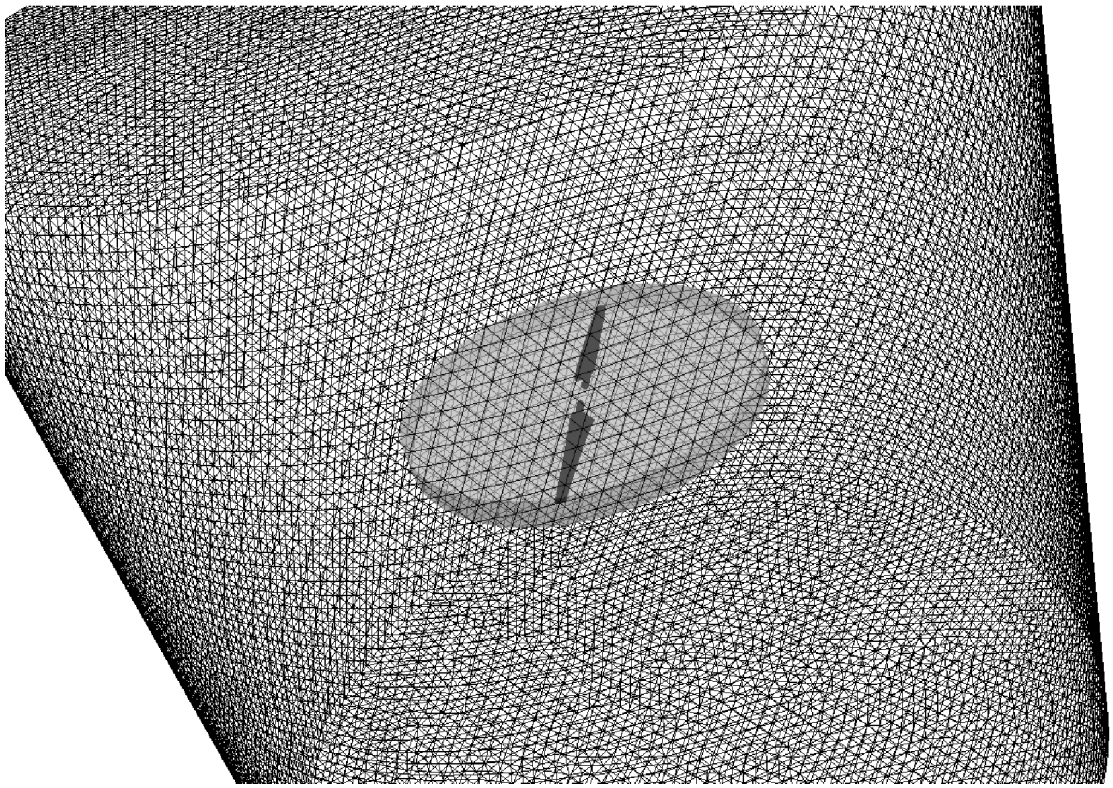

Fig. 10: The virtual interface separating the rotating blades from the rest of the domain

Fig. 11: The used mesh

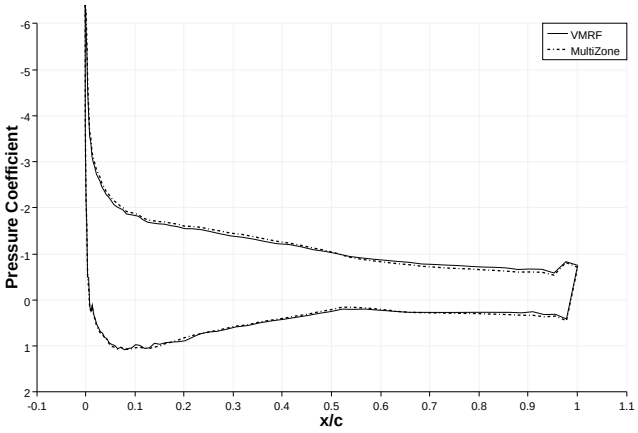

(R/r=0.30)

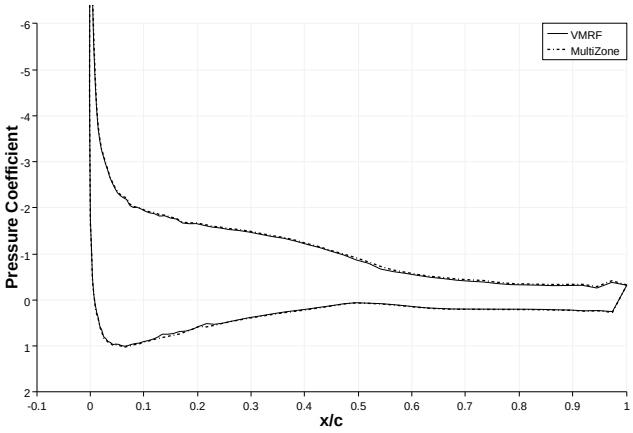

R/r=0.63)

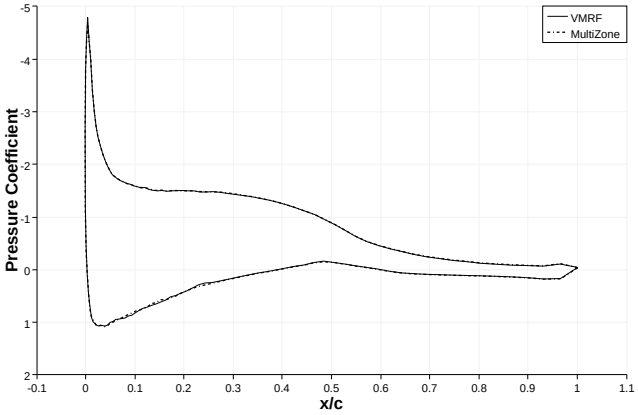

(R/r=0.95)

Fig. 12: Cp profile at different sections of the blade: Comparison VMRF vs MRF

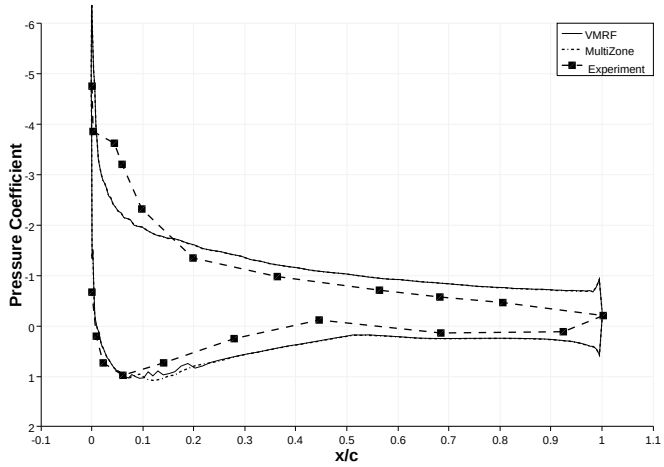

(R/r=0.30%)

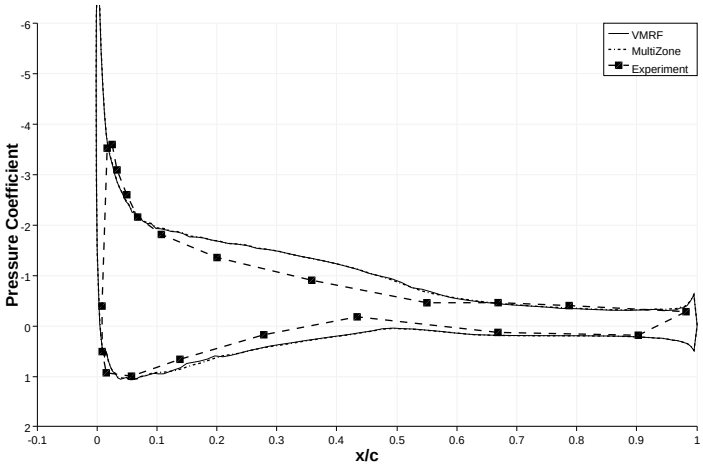

(R/r=0.63)

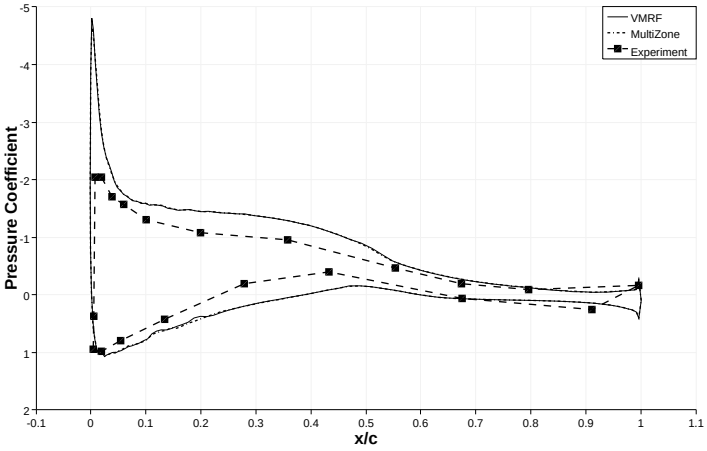

(R/r=0.95%)

Fig. 13: Comparison VMRF vs Experimental data

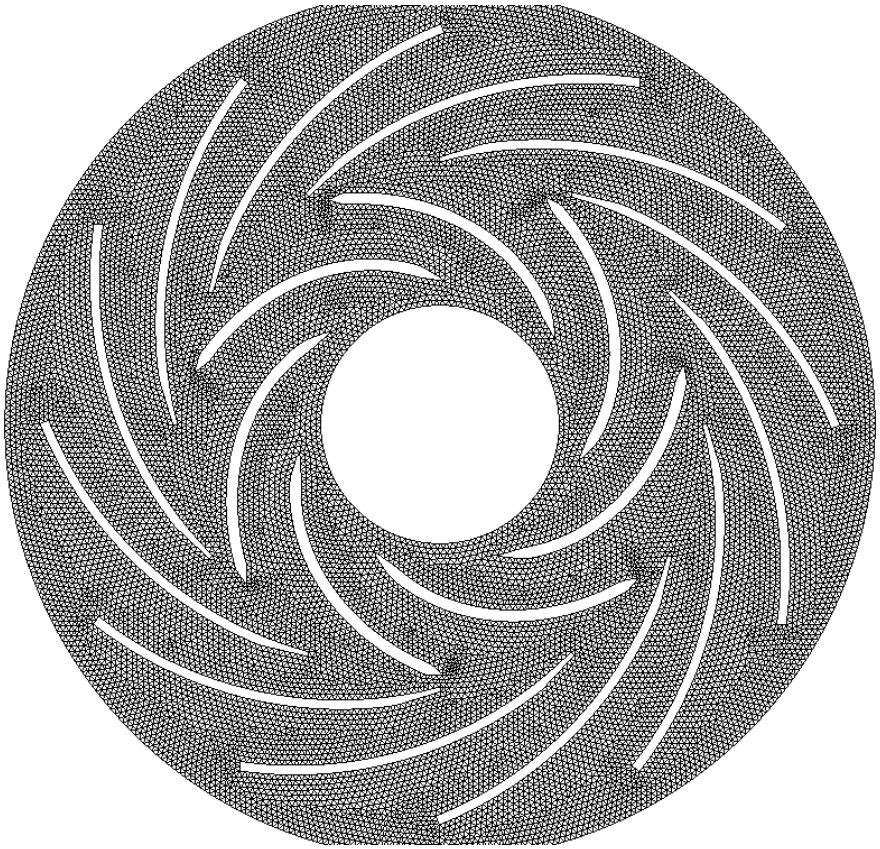

Fig. 14: 2D simplified model of a centifugal pump

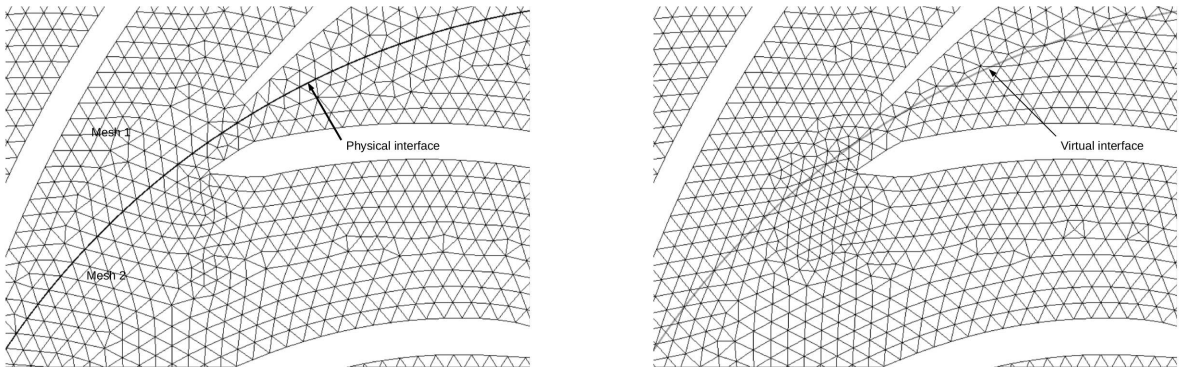

(a) (b)

Fig. 15: Used mesh: (a) two zones MRF mesh, (b) single VMRF mesh

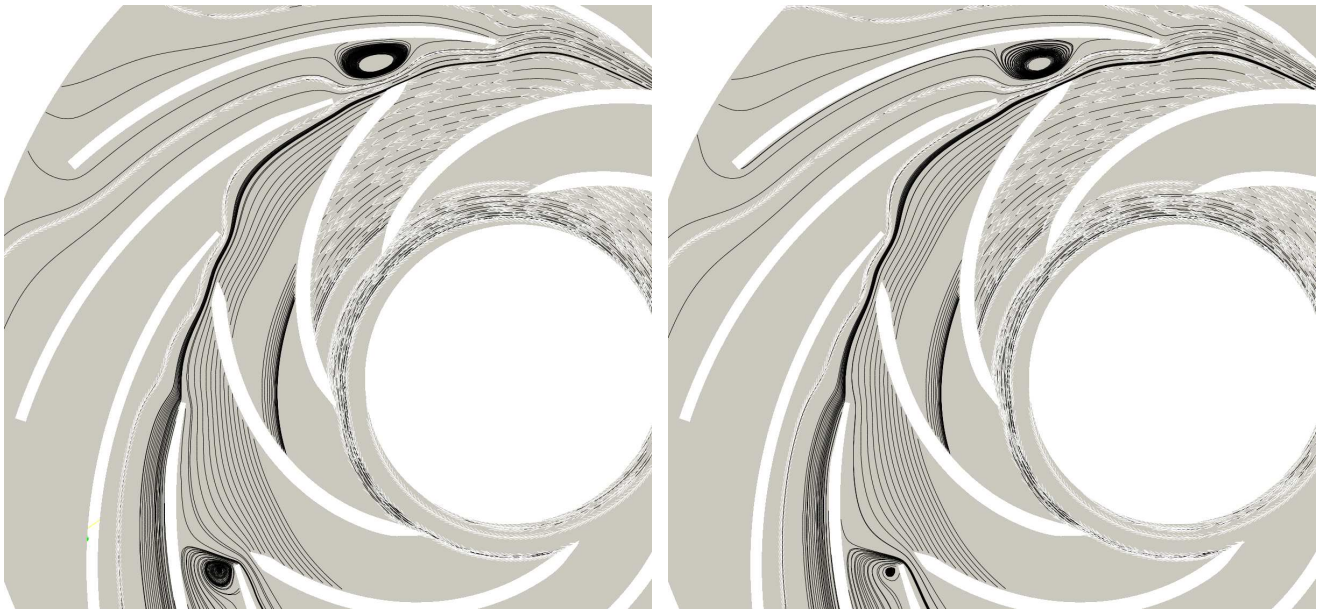

(*a*) (*b*)

Fig. 16: Streamlines on non-matched meshes : (a) MRF results, (b) VMRF results

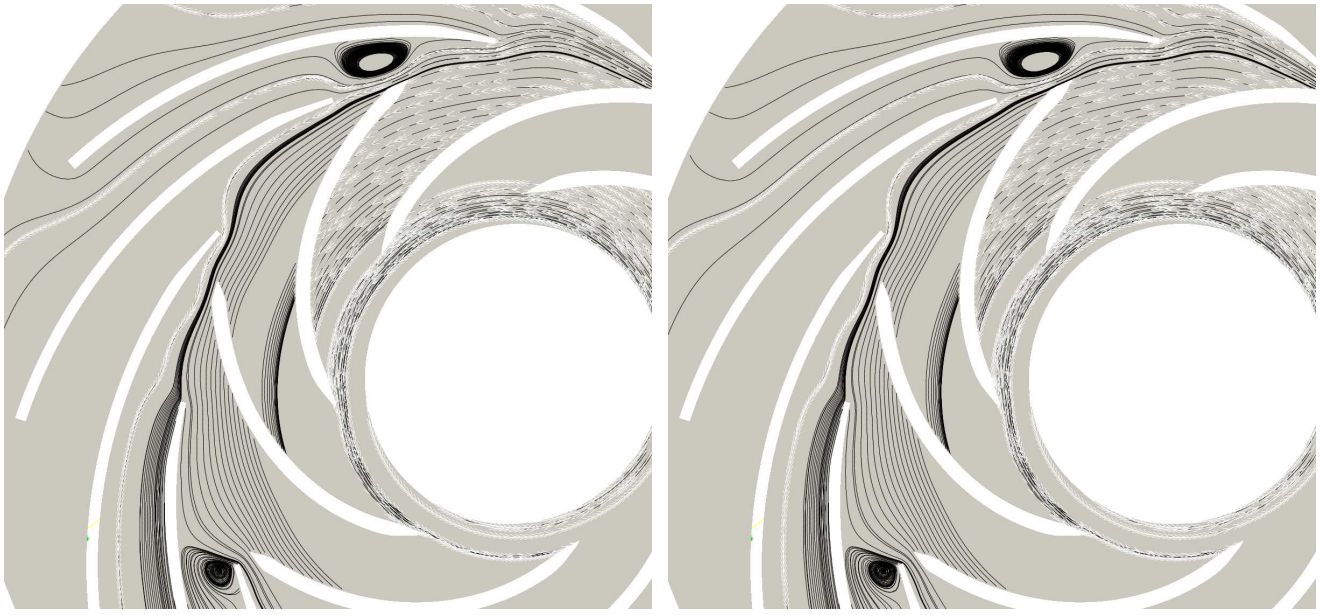

(*a*) (*b*)

Fig. 17: Streamlines on matched meshes : (a) MRF results, (b) VMRF results

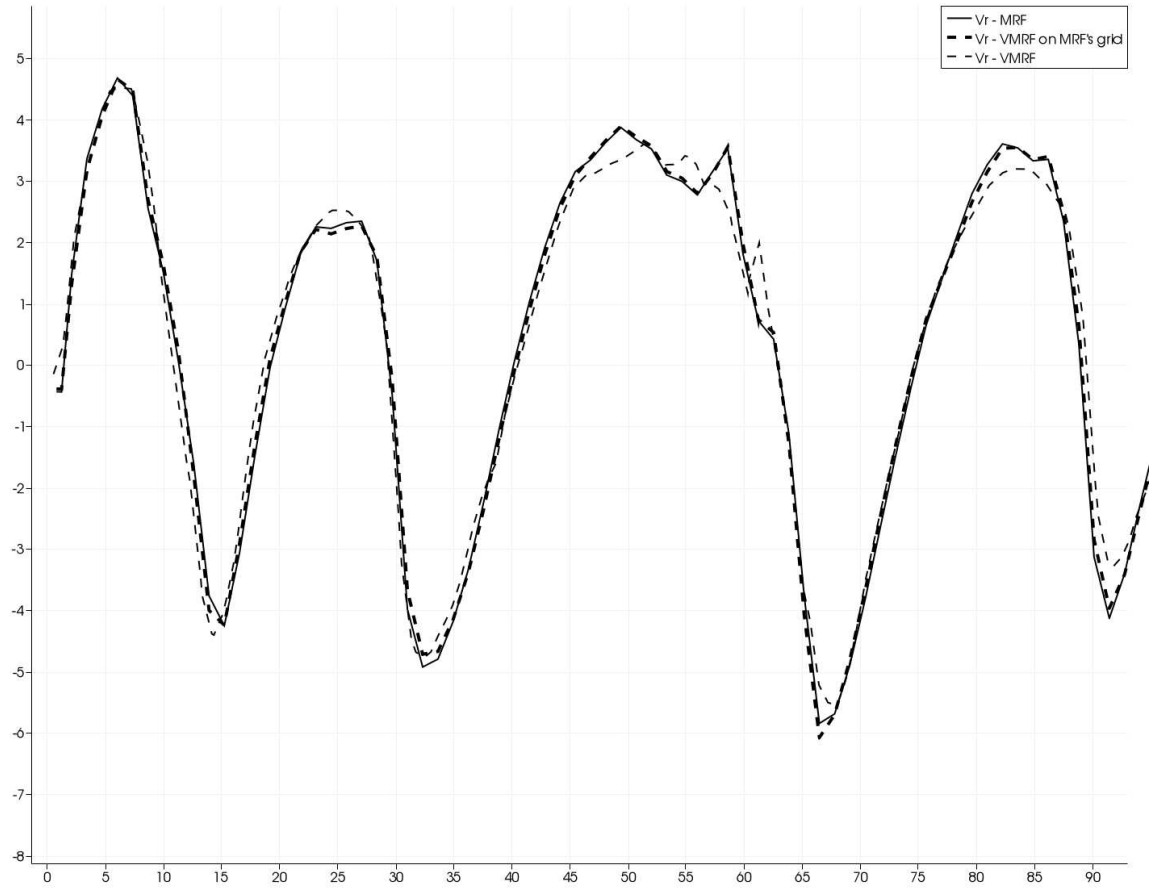

Fig. 18: Pressure profiles comparison along the impeller outlet midspan: VMRF vs MRF